

# PL-UNEXT: PER-STAGE EDGE DETAIL AND LINE FEATURE GUIDED SEGMENTATION FOR POWER LINE DETECTION

Yang Cheng<sup>1</sup>    Zhen Chen<sup>2</sup>    Daming Liu<sup>1</sup>†

<sup>1</sup>Shanghai University of Electric Power, Shanghai 201101, China

<sup>2</sup>State Grid Sichuan Electric Power Research Institute, Chengdu 610041, China

## ABSTRACT

Power line detection is a critical inspection task for electricity companies and is also useful in avoiding drone obstacles. Accurately separating power lines from the surrounding area in the aerial image is still challenging due to the intricate background and low pixel ratio. In order to properly capture the guidance of the spatial edge detail prior and line features, we offer PL-UNeXt, a power line segmentation model with a booster training strategy. We design edge detail heads computing the loss in edge space to guide the lower-level detail learning and line feature heads generating auxiliary segmentation masks to supervise higher-level line feature learning. Benefited from this design, our model can reach 70.6 F1 score (+1.9%) on *TTPLA* and 68.41 mIoU (+5.2%) on *VITL* (without utilizing IR images), while preserving a real-time performance due to few inference parameters.

**Index Terms**— Semantic segmentation, power-line detection, edge detail, line feature, aerial images

## 1. INTRODUCTION

Detecting power lines is a daily inspection task for electric power companies and remains a tough job. Power lines are also safety threats to UAVs but accurately locating them from aerial images is challenging. Power lines usually measure about a few pixels wide in the image, and the very thin shape can be easily fragmented by other objects.

There have been works utilizing traditional computer vision algorithms and deep learning models to detect the power lines. Traditional algorithms suffer a problem of being vulnerable to environment changes and most deep learning models are hard to optimize on such a specialized task. Combining both advantages may be a way to help. Recently, PLGAN [1] was proposed to segment power lines from aerial images. PLGAN developed a generated adversarial network structure with a designed Hough transform loss to embed geometry prior into the model. Choi et al.[2] proposed an attention-based multimodal feature fusion module to utilize both visual images and infrared images and is capable of segmenting power lines in five light and weather conditions.

To further exploit the learning ability of neural network models embedded with prior knowledge in power line detection task, we propose to fully utilize the edge and shape prior of the power lines by guiding the model to learn how to separate edges and extract most relevant line features from the learned edges. Our main contributions are summarized as follows:

- We propose PL-UNeXt, a semantic segmentation model to detect power lines in a real-time speed with booster training strategy to guide the encoder learning edge and line priors.
- Edge detail heads with edge space converter modules are proposed to help the lower-level layers of the encoder generate better edge features.
- Line feature heads with dynamic line extractors are proposed to adaptively assemble multi-sized line features and lead to more appropriate learning representations from the higher-level layers of the encoder.

## 2. RELATED WORK

**Booster Training Strategy.** In real-time semantic segmentation, improving the accuracy of segmentation with same or less inference parameters is challenging. In BiSeNetv2 [3], a booster training strategy is proposed by inserting auxiliary segmentation heads such as rocket boosters to enhance the feature representation in the training phase and discarded in the inference phase. Additionally, Fan et al. [4] proposed STDC with a detail booster branch to guide the lower-level features.

**Line Segment Detection.** Line segment detection has similarity to power line detection, but a major difference is that we only need power lines. AFM [5] adopted the attraction field map to help calculate the line segments. LCNN [6] designed a proposal-sampling-verification process to learn relevant line features. HAWP [7] designed a wire frame parsing algorithm embedded in an end-to-end learning process. F-Clip [8] reformulated the task of detecting center points and line lengths, and customized line detection blocks with bilateral  $7 \times 1$  and  $1 \times 7$  convolutions to exploit line priors.

† Corresponding Author.

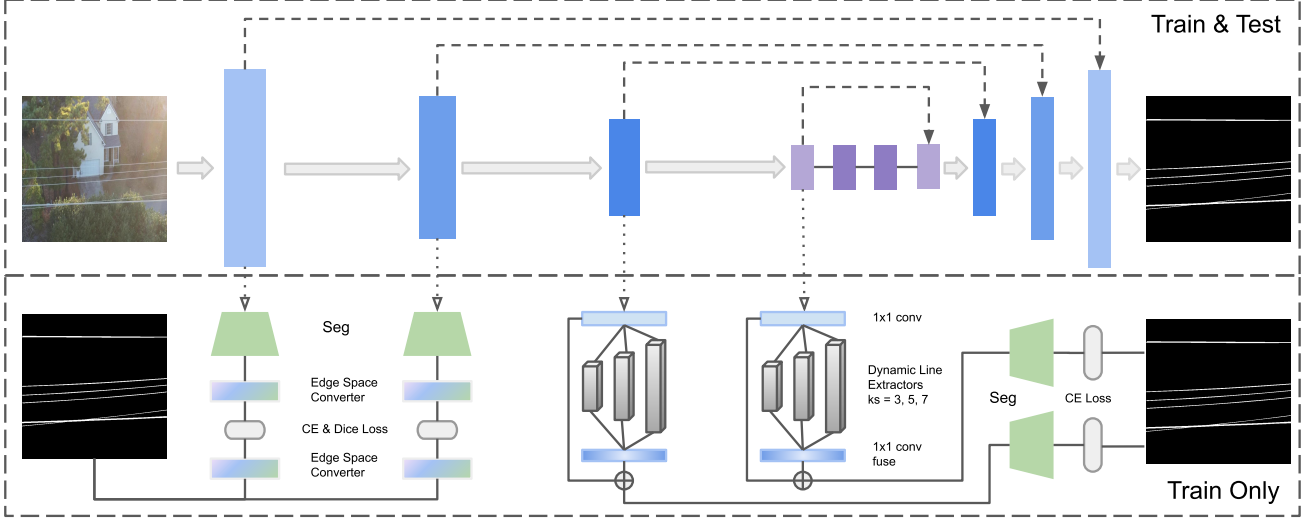


**Fig. 1:** The overview of the PL-UNeXt. The first and second stages of the encoder are guided by the ED heads. The third and fourth stages are guided by the LF heads. The guiding process only exists in the training phase. The Edge Space Converter module and Dynamic Line Extractor module are presented in Fig.2.

### 3. PROPOSED METHOD

To accurately detect power lines in aerial images while maintaining high speed, we propose PL-UNeXt with edge detail guidance and line feature guidance to the encoder stages. As shown in Fig.1, PL-UNeXt can be divided into two parts, train&test part containing a UNeXt [9] encoder-decoder and the training booster part containing also two parts, the edge detail part with two heads and line feature part with the other two heads. As the power lines occupy a small proportion of the image and have strong shape priors like thin, straight, and long, the U-shape network design with a gradually upsample layer by layer is a suitable choice to recover from higher level feature representations and produce fine-grained prediction masks.

#### 3.1. Edge Detail Guidance

In the work of STDC [4], three Laplacian kernels with different strides were used to extract edge detail from the ground truth mask and then compute the loss between the seg logits from the upsampled feature maps and edge details. We explore this further to compute loss in the converted edge space to alleviate the asymmetry between the learned convolution feature maps and edges from the fixed Laplacian convolutions. The STDC used threshold of 0.1 to binarize the edges produced by the Laplacian kernels and the gradient becomes impossible to calculate after the threshold operation, so they apply a fixed  $1 \times 1$  convolution kernel to re-weight the three edge maps of different sizes. Here, we abandon the threshold operation and make the process learnable so that the  $1 \times 1$  convolution we used can learn adaptive weights to fuse the edge maps. Also, we replace the three strided Laplacian kernels

with three non-strided kernels: a Laplacian kernel, a Sobel X kernel, and a Sobel Y kernel to extract more types of edges, thus can enrich the capability of converting to the proper edge space.

Suppose  $X$  as the seg map of the feature maps from the first two stages,  $Y$  as the ground truth, the process can be illustrated as follows:

$$\begin{aligned} \bar{X} &= \text{Cat}(\text{Laplacian}(X), \text{SobelX}(X), \text{SobelY}(X)) \\ \bar{Y} &= \text{Cat}(\text{Laplacian}(Y), \text{SobelX}(Y), \text{SobelY}(Y)) \end{aligned} \quad (1)$$

$$\begin{aligned} \hat{X} &= \text{Softmax}(\text{Norm}(\text{Conv}(\bar{X}))) \\ \hat{Y} &= \text{Softmax}(\text{Norm}(\text{Conv}(\bar{Y}))) \end{aligned} \quad (2)$$

$$\text{Loss} = \alpha(\text{CrossEntropy}(\hat{X}, \hat{Y})) + \beta(\text{Dice}(\hat{X}, \hat{Y})) \quad (3)$$

where  $\alpha$  and  $\beta$  are super parameters and set to 1.0 and 0.4.

#### 3.2. Line Feature Guidance

After processed by the lower-level layers guided by the edge detail prior, higher-level layers need to focus more on the real object we need to separate, the power lines. As shown in Fig.1, the third and fourth stages of the encoder are guided by two line feature heads which extract the line features and compute the seg loss with the ground truth labels. In the work of F-Clip [8], a custom line detection block with two parallel convolutions with kernel sizes of  $1 \times 7$  and  $7 \times 1$ . We extend this design further to expand the capacity and flexibility of extracting the lines. The main functional part of the line feature heads is composed of three dynamic line extractors with different kernel sizes and a  $1 \times 1$  convolution to fuse the extracted features. In dynamic line extractors, we adopt Dynamic Convolution [15] to increase extractor capability without significant growth of training parameters. In each dynamic line extractor, the feature maps are bilaterally

Models	Modality	Original	Day	Fog	Night	Snow	Average	Param (M)	Fps
UNet [10]	VL	60.09	57.96	56.93	55.20	57.50	57.53	31.04	32.9
UNet+EF [11]	IR+VL	59.51	57.99	55.91	53.65	57.30	56.87	31.04	32.7
UNet+EF+SE [12]	IR+VL	61.13	59.75	57.56	56.33	59.55	58.84	32.44	24.9
UNet+FuseNet [13]	IR+VL	60.77	59.32	57.57	55.62	58.57	58.37	12.48	22.3
UNet+MMTM [14]	IR+VL	60.95	59.61	58.08	57.39	59.20	59.04	13.53	14.5
UNet+FFM [2]	IR+VL	61.71	60.89	59.00	58.00	60.59	60.03	12.73	8.5
UMFNet [2]	IR+VL	63.31	62.47	61.59	61.14	61.57	62.01	15.70	26.0
UMFNet+FuseNet	IR+VL	62.85	62.05	60.79	60.47	61.53	61.54	15.70	26.1
UMFNet+MMTM	IR+VL	63.65	62.92	62.28	61.63	62.31	62.56	16.40	18.5
UMFNet+FFM [2]	IR+VL	64.07	63.72	62.65	62.60	63.01	63.21	15.92	11.0
Ours	VL	<b>70.43</b>	<b>70.15</b>	<b>69.57</b>	<b>62.62</b>	<b>69.27</b>	<b>68.41</b>	1.47(6.39)	87.8

**Table 1:** The mIoU results (%) comparison on VITL dataset [2] with same image size of  $256 \times 256$ . The VL and IR in the Modality column means *visible light* and *infrared*. VL indicates that the model used visible image only and IR+VL indicates that the model used both visible image and infrared image. The Ours param number outside the brackets is for the inference stage and the number in the brackets is for the training stage.

processed by two Dynamic Convolutions with kernel size of  $1 \times N$  and  $N \times 1$ , where  $N$  is different kernel sizes we set to dynamic line extractors. Then the feature maps are concatenated and processed by  $1 \times 1$  convolution to merge the feature maps in an adaptive way. Let  $X$  be the input feature maps, the process can be illustrated as follows:

$$Feat = Cat(DyConvX(X), DyConvY(X)) \quad (4)$$

$$Out = Act(Norm(Conv(Feat))) \quad (5)$$

The outputs of the dynamic line extractors are fused by  $1 \times 1$  convolution and concatenated with the original feature maps. Then the final outputs are used to generate train-only predictions to calculate the auxiliary segmentation loss.

### 3.3. Optimization with Auxiliary Loss

Our proposed booster strategy exists only in the training phase and all boosters are discarded in the testing phase. During training, the losses of the booster heads will conduct the gradient to the backbone of the model which exists all time. The overall loss during training is as follows:

$$L = \theta L_{decode} + \iota L_{ED1} + \kappa L_{ED2} + \lambda L_{LF1} + \mu L_{LF2} \quad (6)$$

where  $\theta$ ,  $\iota$ ,  $\kappa$ ,  $\lambda$  and  $\mu$  are all set to 1.0.

## 4. EXPERIMENTS

### 4.1. Implementation Details

**Dataset and Metric.** We evaluate our method on TTPLA and VITL following the settings of PLGAN[1] and UMFNet[2] and also compare the results with them as baselines. We adopt F1 score, Precision, Recall and IoU for the evaluation on TTPLA, and mIoU for the test on VITL, following the way they presented.

**Settings and Platform.** To train our model, we choose AdamW as the optimizer with an initial learning rate of 0.0005 and weight decay of 0.05. We use CosineAnnealing policy with a minimum learning rate of  $5e-6$  to find more

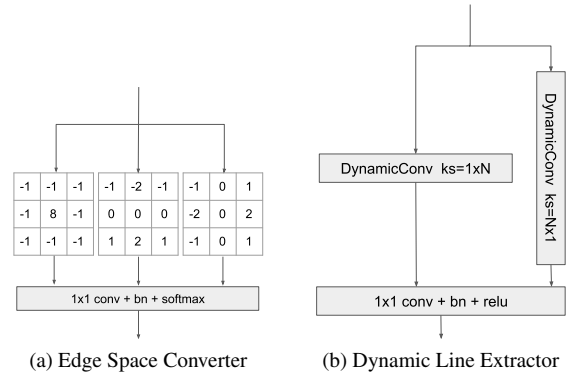


**Fig. 2:** Structure of the sub-modules.

optimal minima. Our method is implemented on Pytorch and the experiments are run on NVIDIA GeForce RTX 3050.

### 4.2. Experimental Results

**TTPLA.** As shown in Tab.2, our PL-UNeXt outperforms PLGAN with minor superiority. The F1 score and IoU improves by 1.9% and 1.3%. The Precision rate of PLGAN is still the highest but our Recall rate outperforms by 5.7%, contributing to a more balanced detecting performance.

**VITL.** Considering not all UAVs are equipped with infrared cameras, our model is proposed to a more generalized scene with regular cameras so we use visible images only. As shown in Tab.1, our model outperforms by 5.2% mIoU in the average value of the five light and weather conditions preserving the highest fps.

**Visualization.** We visualize the feature maps produced by stage 3 of the encoder and final prediction masks in Fig.3. The visualizations compare the results produced without and with edge detail and line feature guidance. The feature maps show that the weights are more focused and neat on the power

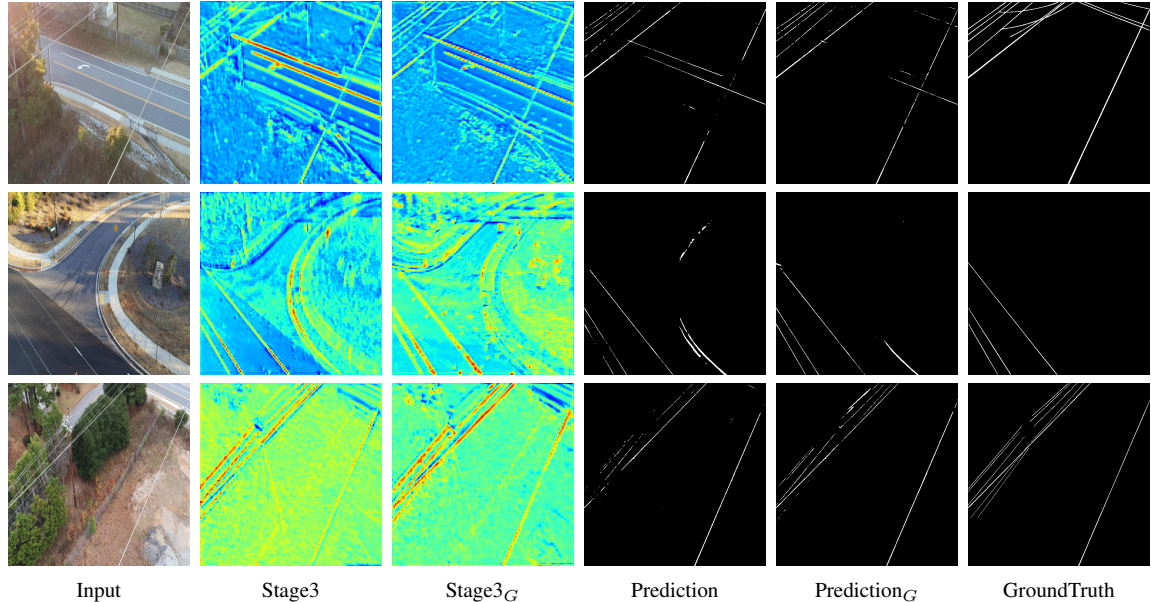


**Fig. 3:** Visual comparison of the feature maps and predictions on TTPLA. The subscript  $G$  denotes results with guidance of our designed edge detail and line feature heads.

lines, thus contributing to predictions closer to ground truths and less false positives.

Models	$F_1$	IoU	Pre.	Rec.	P (M)
FPN [16]	0.569	0.423	0.769	0.513	23.2
UNET [10]	0.662	0.515	0.846	0.583	24.4
UNET++ [17]	0.668	0.522	0.843	0.591	26.1
Pix2pix [18]	0.663	0.509	0.822	0.577	10.6
GcGAN [19]	0.655	0.501	0.837	0.556	13.4
AFM [5]	0.457	0.307	0.495	0.432	44.0
LCNN [6]	0.498	0.315	0.541	0.464	10.9
HAWP [7]	0.485	0.315	0.581	0.421	11.6
PLGAN [1]	0.687	0.533	<b>0.863</b>	0.577	14.9
Ours	<b>0.706</b>	<b>0.546</b>	0.821	<b>0.634</b>	1.5

**Table 2:** PL segmentation performance of the proposed and the comparison methods on TTPLA dataset [20]. Following previous works, models are evaluated on the images and labels resized to  $512 \times 512$ . The number of params is for inference stage.

### 4.3. Ablation Study

To prove the effectiveness of our designed ED and LF, we separately added ED and LF heads on the first two stages and the last two stages of the encoder. The results are presented in Tab.3 and can be seen that the ED and LF achieved 1.1% F1 and 1.4% F1 score improvements, also 1.2% and 1.6% improvements on IoU. Altogether the two ED and LF contributed the final proposed model and reached higher accuracy. The visualization comparison in Fig.3 clearly shows that our ED and LF can help guide the encoder by focusing

on more relative line shapes and producing more precise predictions.

Methods	$F_1$	IoU
Base	0.683	0.519
Base + ED	0.694	0.531
Base + LF	0.697	0.535
Base + ED + LF	0.706	0.546

**Table 3:** Ablation study of the methods on TTPLA dataset [20]. Here the Base is the UNeXt network, ED is the proposed edge detail head and LF is the proposed line feature head.

## 5. CONCLUSION

In this work, we propose PL-UNeXt with a booster training strategy to maximize edge and shape prior knowledge in power line segmentation. We first propose two edge detail heads to guide the lower-level layers of the encoder to learn better edge proposals, then we propose two line feature heads to guide the higher-level layers of the encoder by adaptively extracting and verifying the relevant line feature representations. Extensive experiments show that PL-UNeXt outperforms recently proposed methods. Visualizations show that our design is reasonable to fit the need of our envisage.

## 6. REFERENCES

- [1] Rabab Abdelfattah, Xiaofeng Wang, and Song Wang, “Plgan: Generative adversarial networks for power-line segmentation in aerial images,” *arXiv preprint arXiv:2204.07243*, 2022.
- [2] Hyeeyeon Choi, Jong Pil Yun, Bum Jun Kim, Hyeonah Jang, and Sang Woo Kim, “Attention-based multimodal image feature fusion module for transmission line detection,” *IEEE Transactions on Industrial Informatics*, vol. 18, no. 11, pp. 7686–7695, 2022.
- [3] Changqian Yu, Changxin Gao, Jingbo Wang, Gang Yu, Chunhua Shen, and Nong Sang, “Bisenet v2: Bilateral network with guided aggregation for real-time semantic segmentation,” *International Journal of Computer Vision*, vol. 129, pp. 3051–3068, 2021.
- [4] Mingyuan Fan, Shenqi Lai, Junshi Huang, Xiaoming Wei, Zhenhua Chai, Junfeng Luo, and Xiaolin Wei, “Rethinking bisenet for real-time semantic segmentation,” in *Proceedings of the IEEE/CVF Conference on Computer Vision and Pattern Recognition*, 2021, pp. 9716–9725.
- [5] Nan Xue, Song Bai, Fudong Wang, Gui-Song Xia, Tianfu Wu, and Liangpei Zhang, “Learning attraction field representation for robust line segment detection,” in *IEEE/CVF Conference on Computer Vision and Pattern Recognition (CVPR)*, 2019, pp. 1595–1603.
- [6] Yichao Zhou, Haozhi Qi, and Yi Ma, “End-to-End wireframe parsing,” in *IEEE/CVF International Conference on Computer Vision (ICCV)*, 2019, pp. 962–971.
- [7] Nan Xue, Tianfu Wu, Song Bai, Fudong Wang, Gui-Song Xia, Liangpei Zhang, and Philip HS Torr, “Holistically-attracted wireframe parsing,” in *IEEE/CVF Conference on Computer Vision and Pattern Recognition (CVPR)*, 2020, pp. 2788–2797.
- [8] Xili Dai, Haigang Gong, Shuai Wu, Xiaojun Yuan, and Ma Yi, “Fully convolutional line parsing,” *Neurocomputing*, vol. 506, pp. 1–11, 2022.
- [9] Jeya Maria Jose Valanarasu and Vishal M Patel, “Unext: Mlp-based rapid medical image segmentation network,” in *Medical Image Computing and Computer Assisted Intervention—MICCAI 2022: 25th International Conference, Singapore, September 18–22, 2022, Proceedings, Part V*. Springer, 2022, pp. 23–33.
- [10] Olaf Ronneberger, Philipp Fischer, and Thomas Brox, “U-net: Convolutional networks for biomedical image segmentation,” in *International Conference on Medical image computing and computer-assisted intervention*. Springer, 2015, pp. 234–241.
- [11] Hyeeyeon Choi, Gyogwon Koo, Bum Jun Kim, and Sang Woo Kim, “Real-time power line detection network using visible light and infrared images,” in *2019 International Conference on Image and Vision Computing New Zealand (IVCNZ)*. IEEE, 2019, pp. 1–6.
- [12] Jie Hu, Li Shen, and Gang Sun, “Squeeze-and-excitation networks,” in *Proceedings of the IEEE conference on computer vision and pattern recognition*, 2018, pp. 7132–7141.
- [13] Caner Hazirbas, Lingni Ma, Csaba Domokos, and Daniel Cremers, “Fusenet: Incorporating depth into semantic segmentation via fusion-based cnn architecture,” in *Computer Vision—ACCV 2016: 13th Asian Conference on Computer Vision, Taipei, Taiwan, November 20–24, 2016, Revised Selected Papers, Part I 13*. Springer, 2017, pp. 213–228.
- [14] Hamid Reza Vaezi Joze, Amirreza Shaban, Michael L Iuzzolino, and Kazuhito Koishida, “Mmtm: Multimodal transfer module for cnn fusion,” in *Proceedings of the IEEE/CVF Conference on Computer Vision and Pattern Recognition*, 2020, pp. 13289–13299.
- [15] Yinpeng Chen, Xiyang Dai, Mengchen Liu, Dongdong Chen, Lu Yuan, and Zicheng Liu, “Dynamic convolution: Attention over convolution kernels,” in *Proceedings of the IEEE/CVF conference on computer vision and pattern recognition*, 2020, pp. 11030–11039.
- [16] Tsung-Yi Lin, Piotr Dollár, Ross Girshick, Kaiming He, Bharath Hariharan, and Serge Belongie, “Feature pyramid networks for object detection,” in *IEEE Conference on Computer Vision and Pattern Recognition (CVPR)*, 2017, pp. 2117–2125.
- [17] Zongwei Zhou, Md Mahfuzur Rahman Siddiquee, Nima Tajbakhsh, and Jianming Liang, “Unet++: A nested unet architecture for medical image segmentation,” in *Deep learning in medical image analysis and multimodal learning for clinical decision support*, pp. 3–11. Springer, 2018.
- [18] Phillip Isola, Jun-Yan Zhu, Tinghui Zhou, and Alexei A Efros, “Image-to-image translation with conditional adversarial networks,” in *IEEE Conference on Computer Vision and Pattern Recognition (CVPR)*, 2017, pp. 1125–1134.
- [19] Huan Fu, Mingming Gong, Chaohui Wang, Kayhan Batmanghelich, Kun Zhang, and Dacheng Tao, “Geometry-consistent generative adversarial networks for one-sided unsupervised domain mapping,” in *IEEE Conference on Computer Vision and Pattern Recognition (CVPR)*, 2019, pp. 2427–2436.
- [20] Rabab Abdelfattah, Xiaofeng Wang, and Song Wang, “Ttpla: An aerial-image dataset for detection and segmentation of transmission towers and power lines,” in *Proceedings of the Asian Conference on Computer Vision*, 2020.